Harmonic Analysis of Time-Series AVHRR NDVI Data

Mark E. Jakubauskas, David R. Legates, and Jude H. Kastens

Abstract

Harmonic analysis of a one-year time series (26 periods) of NOAA AVHRR NDVI biweekly composite data was used to characterize seasonal changes for natural and agricultural land use/land cover in Finney County in southwest Kansas. Different crops (corn, soybeans, alfalfa) exhibit distinctive seasonal patterns of NDVI variation that have strong periodic characteristics. Harmonic analysis, also termed spectral analysis or Fourier analysis, decomposes a time-dependent periodic phenomenon into a series of sinusoidal functions, each defined by unique amplitude and phase values. The proportion of variance in the original time-series data set accounted for by each term of the harmonic analysis can also be calculated. Amplitude and phase angle images were produced from analysis of the time-series NDVI data and correlated with information on crop type and extent for the region to develop a methodology for crop-type identification. Crop types occurring in southwest Kansas, including corn, winter wheat, alfalfa, pasture, and native prairie grasslands, were characterized and identified using this technique and biweekly AVHRR composite data for 1992. For crops with a simple phenology, such as corn, the majority of the variance was captured by the first and additive terms of the harmonic analysis, while winter wheat exhibited a bimodal NDVI periodicity with the majority of the variance accounted for by the second harmonic term.

Introduction

Recent advances in remote sensing technology and theory have expanded opportunities to characterize the seasonal and interannual dynamics of natural and managed vegetation communities. Studies have shown that the temporal domain of multispectral data frequently provides more information about vegetation cover and condition than the spatial, spectral, or radiometric domains (Briggs and Nellis, 1991; Kremer and Running, 1993; Eastman and Fulk, 1993; Samson, 1993; Reed *et al.*, 1994). Time series analysis of Advanced Very High Resolution Radiometer (AVHRR) multispectral imagery has allowed scientists to examine regional- to global-scale phenological phenomena such as greenup, duration of green period, onset of senescence, and changes in seasonally dependent biophysical variables such as leaf area index (LAI), biomass, and net primary productivity (Tucker *et al.*, 1985; Roller and Colwell, 1986; Achard and Brisco, 1990; Eastman and Fulk, 1993; Reed *et al.*, 1994; Lancaster *et al.*, 1996; Myneni *et al.*, 1997).

Approaches to the analysis of time series remotely sensed imagery have varied considerably, from standardized principal component analysis (Eastman and Fulk, 1993), to textural analysis (Briggs and Nellis, 1991), to the development of phenological metrics that describe seasonal changes in the normalized difference vegetation index (NDVI) (Lloyd, 1990; Samson, 1993; Reed *et al.*, 1994). While metrics defined by Lloyd and Reed *et al.* are excellent descriptions of a particular time-series phenomenon and have found general acceptance and application in ecology and agriculture (Loveland *et al.*, 1995; Reed *et al.*, 1996; Kastens *et al.*, 1997; Reed and Yang, 1997; Tieszen *et al.*, 1997;), they do not represent a true time-series analyses, defining instead the *characteristics* of a time-series phenomenon (e.g., the height, magnitude, duration, or area of the time-series curve).

In this paper, we describe the application of harmonic analysis (also known as Fourier analysis) to a 26-period time series of NOAA-AVHRR NDVI biweekly composite NDVI data of Finney County, Kansas. We discuss the theory behind harmonic analysis (HA) of time series, some applications of one- and two-dimensional harmonic analysis of time-series data in other research fields, and the application of HA specifically to a time-series of satellite imagery. Within the scope of this paper, we discuss only the application of the HA to a single year of NOAA-AVHRR data (26 periods), focusing on five specific land-use/land-cover types common to the study area (irrigated corn, winter wheat, irrigated alfalfa, native shortgrass prairie, and native sandsage prairie as case examples of the harmonic analysis applied to time-series imagery.

Overview of Harmonic Analysis

Briefly defined, harmonic (Fourier) analysis permits a complex curve to be expressed as the sum of a series of cosine waves (terms) and an additive term (Rayner, 1971; Davis, 1986). Each wave is defined by a unique amplitude and a phase angle, where the amplitude value is half the height of a wave, and the phase angle (or simply, phase) defines the offset between the origin and the peak of the wave over the range 0 to 2π (Figure 1a). Each term designates the number of complete cycles completed by a wave over the defined interval (e.g., the second term completes two cycles) (Figure 1b). Successive harmonic terms are added to produce a complex curve (Figure 1c), and each component curve, or term, accounts for a percentage of the total variance in the original time-series data set. Fourier analysis has been used in digital image processing for analysis of a single image as a two-dimensional wave form (Jensen, 1996; Schowengerdt, 1997), and more recently has been used for analyzing sets of successive regular multidate samples of satellite remotely sensed imagery (Andres *et al.*, 1994; Olsson and Eklundh, 1994; Verhoef *et al.*, 1996; Azzali and Menenti, 2000).

M.E. Jakubauskas and J.H. Kastens are with the Kansas Applied Remote Sensing (KARS) Program, University of Kansas, Lawrence, KS 66045 (mjakub@eagle.cc.ukans.edu)

D.R. Legates is with the Department of Geography, University of Delaware, Newark, DE 19716-2541.

Photogrammetric Engineering & Remote Sensing
Vol. 67, No. 4, April 2001, pp. 461–470.

0099-1112/01/6704–461$3.00/0

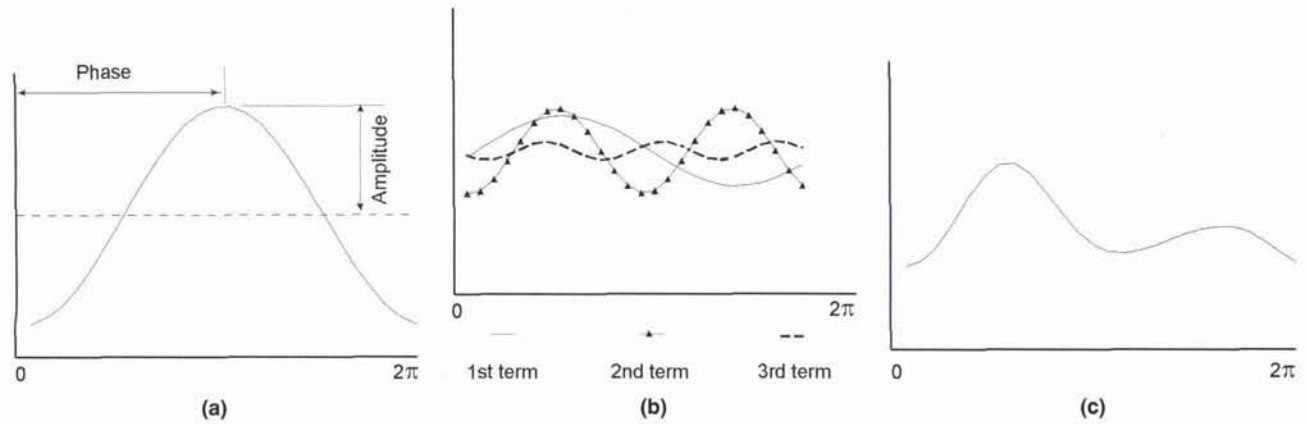

Figure 1. (a) Simple cosine curve representative of the first harmonic. (b) Curves for harmonic terms 1, 2, and 3. (c) Curve produced from addition of curves in Figure 1b.

Mathematical Definition of Harmonic Analysis

Fourier series analysis decomposes a signal into an infinite series of harmonic components. Each of these components is comprised initially of a sine wave and a cosine wave of equal integer frequency. These two waves are then combined into a single cosine wave, which has characteristic amplitude (size of the wave) and phase angle (offset of the wave). Convergence has been established for bounded piecewise continuous functions on a closed interval, with special conditions at points of discontinuity. Its convergence has been established for other conditions as well, but these are not relevant to the analysis at hand. For simplicity, the following write-up is for functions which are continuous in the closed interval $[0,L]$, but these results can easily be generalized to piecewise continuous functions. In this paper, $L = 26$, because there are 26 biweekly composite periods in the 1992 data set, and any period x (1 to 26) occurs in that data set.

Let $f(x)$ be a continuous function on $[0,L]$. Then

$$f(x) = \sum_{n=1}^{\infty} \left(a_n \cos \frac{2\pi nx}{L} + b_n \sin \frac{2\pi nx}{L} \right) + \frac{1}{2} a_0. \qquad (1)$$

The right hand side is the *Fourier series* representation for $f(x)$.

By the orthogonality properties of sine and cosine, the above equation can be manipulated (multiplied by a function and integrated) twice to yield the following equations for a_n and b_n, the coefficients of the Fourier series:

$$a_n = \frac{2}{L} \int_0^L f(x) \cos \frac{2\pi nx}{L} \, dx \qquad \text{for } n \geq 0 \qquad (2)$$

$$b_n = \frac{2}{L} \int_0^L f(x) \sin \frac{2\pi nx}{L} \, dx \qquad \text{for } n \geq 0 \qquad (3)$$

Note that $b_0 = 0$ and $\frac{1}{2} a_0 = \frac{1}{L} \int_0^L f(x) \, dx$, which is actually the function average for $f(x)$. With the coefficients as defined above, the Fourier series is unique (i.e., if two Fourier series describe a function, then it can be shown that corresponding coefficients of the two series must be equal and hence the two series are the same).

Define the jth harmonic to be the jth term in the Fourier series (for $j \geq 1$), given by

$$a_j \cos \frac{2\pi jx}{L} + b_j \sin \frac{2\pi jx}{L}.$$

The jth harmonic can be converted to a single cosine term as follows:

$$\begin{aligned} & a_j \cos \frac{2\pi jx}{L} + b_j \sin \frac{2\pi jx}{L} \\ &= \sqrt{a_j^2 + b_j^2} \left(\frac{a_j}{\sqrt{a_j^2 + b_j^2}} \cos \frac{2\pi jx}{L} + \frac{b_j}{\sqrt{a_j^2 + b_j^2}} \sin \frac{2\pi jx}{L} \right) \\ &= \sqrt{a_j^2 + b_j^2} \left(\cos \phi_j \cos \frac{2\pi jx}{L} + \sin \phi_j \sin \frac{2\pi jx}{L} \right) \\ &= c_j \cos \left(\frac{2\pi jx}{L} - \phi_j \right), \end{aligned}$$

where $c_j = \sqrt{a_j^2 + b_j^2}$ is the length of the vector $\langle a_j, b_j \rangle$ in the xy-plane, and $\phi_j = \arctan \frac{b_j}{a_j}$ is the angle (direction) of the vector $\langle a_j, b_j \rangle$ in the xy-plane. Because the inverse tangent function only returns values in the interval $\left[-\frac{\pi}{2}, \frac{\pi}{2} \right]$, whenever $a_j < 0$ the modified definition $\phi_j = \arctan \frac{b_j}{a_j} + \pi$ must be used to obtain a true phase angle. It follows that $\phi_j \in \left[-\frac{\pi}{2}, \frac{3\pi}{2} \right]$. If c_0 is defined to be $\frac{1}{2} a_0$, we have the following:

$$f(x) = c_0 + \sum_{n=1}^{\infty} c_n \cos \left(\frac{2\pi nx}{L} - \phi_n \right), \qquad (4)$$

where c_n is the *amplitude* of the nth term (which is the nth harmonic), and ϕ_n is the *phase angle* of the nth term.

For a finite data set $\{y(k); k = 1, 2, \ldots, N\}$, a finite technique that does not involve integrals is needed. Define the following:

$$a_j = \frac{1}{N-1}\left(y(1) + y(N) + 2\sum_{k=2}^{N-1} y(k)\cos\frac{2\pi j(k-1)}{N-1}\right) \text{ for } j \geq 0 \quad (5)$$

$$b_j = \frac{1}{N-1}\left(2\sum_{k=2}^{N-1} y(k)\sin\frac{2\pi j(k-1)}{N-1}\right) \text{ for } j \geq 1 \quad (6)$$

These are the trapezoidal approximations to the Equations 2 and 3 defined above.

$$\text{Trapezoid rule: } \int_0^L f(x)dx \approx \frac{\Delta x}{2}\left(f(0) + f(L) + 2\sum_{k=1}^{n-1} f(k\Delta x)\right),$$

where $\Delta x = \frac{L}{n}$.

$$\Delta x = 1 \Rightarrow \int_0^L f(x)\,dx \approx \frac{1}{2}\left(f(0) + f(L) + 2\sum_{k=1}^{n-1} f(k)\right)$$

Equations 5 and 6 can be evaluated numerically to acquire the Fourier coefficients for each term, which can then be used to calculate amplitudes and phase angles for each of the harmonic components.

Applications of Harmonic Analysis to Environmental Phenomena

One-dimensional harmonic analysis of time-series data has found widespread application in the geosciences, including geology (varve sequences), oceanography (tidal patterns), and hydrology (runoff and stream flow)(Anderson and Koopmans, 1963; Rayner, 1971; Yevjevich, 1972; Schulz and Stattegger, 1997). The two-dimensional extension of harmonic analysis adds spatial pattern to the temporal data stream and has found significant application in meteorology and climatology. Van Loon *et al.* (1973), for example, used harmonic analysis to describe zonal standing waves in the atmosphere—pressure waves that describe the ridges and troughs exhibited by the isobars on weather maps. Their analysis indicated that the first three harmonic terms (up to three ridges and troughs around the globe) were sufficient to explain nearly all of the large-scale latitudinal variations in pressure. Heddinghaus and Kung (1980) similarly used harmonic analysis, in combination with principal components analysis, to investigate mean patterns of circulation in the Northern Hemisphere. They also concluded that most of the variability in atmosphere pressure could be explained by the first three harmonic terms. Legates and Willmott (1990b) further employed harmonic analysis to explain seasonal trends in global surface air temperature. Their analysis clearly delineates areas that exhibit a strong seasonal cycle in air temperature (i.e., the middle and upper latitudes) from areas where air temperature has a strong biannual cycle (i.e., equatorial regions).

The most widespread use of harmonic analysis in the geosciences has been to examine precipitation patterns and thunderstorm frequencies. For example, Horn and Bryson (1960) represented the observed precipitation curve for Madison, Wisconsin using six harmonics. These harmonics then were used to help explain the more complex precipitation patterns exhibited by the raw data. Wallace (1975), Hamilton (1981), Balling (1985), Landin and Bosart (1985), Landin and Bosart (1989), Riley *et al.* (1987), and Legates and Willmott (1990a) all have successfully applied harmonic analysis to describing and representing precipitation patterns. In addition, harmonic analysis has been widely used to investigate thunderstorm frequencies and to help explain diurnal patterns of thunderstorm occurrence. Rasmusson (1971), Wallace (1975), Easterling and Robinson (1985), and Masò (1991), for example, used harmonic analysis to describe the characteristics of afternoon, evening, and nocturnal thunderstorm dynamics for various regions of the United States. By examining the phase shift and the amplitude of the various harmonic terms, these researchers were able to describe the spatial variability in various patterns of thunderstorm activity. Clearly, harmonic analysis has proven useful with data that exhibit relatively abrupt changes, because precipitation and thunderstorm frequency data rarely are smooth fields. Harmonic analysis is useful in that seasonal and intraseasonal cycles can be highlighted and offers great promise for analyzing seasonal and interannual variation in land surface condition as recorded by NDVI values calculated from time-series remotely sensed data such as the AVHRR.

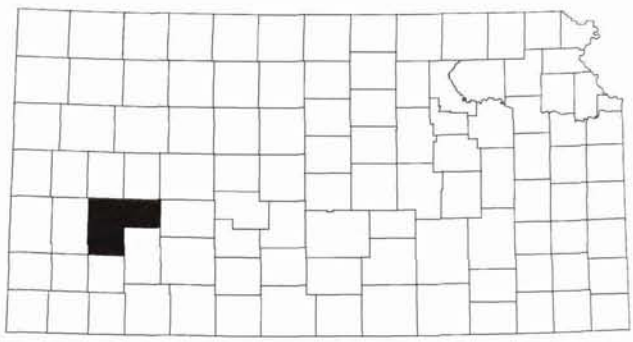

Figure 2. Finney County locator map.

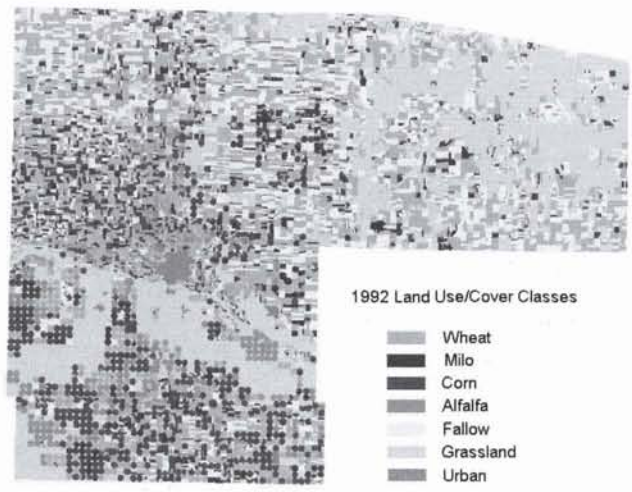

Figure 3. Finney County 1992 land-use/land-cover map, from Egbert *et al.* (1995).

Methodology

Study Area: Finney County, Kansas

Finney County, the second-largest county in Kansas at approximately 1300 square miles (3366 sq km), is located in southwestern Kansas in the High Plains at approximately 100°W longitude (Figure 2). Cropland dominates the relatively flat landscape of Finney County, comprising over 76 percent of the county (Figure 3). The Arkansas River extends east-west through the central portion of the county, and irrigated agriculture (predominantly corn, milo, and alfalfa) is clustered along

the river, drawing on the Ogalalla Aquifer to supply center-pivot irrigation systems. Dryland agriculture dominates the northern and southern parts of the county, with winter wheat as the principal crop. Some native shortgrass prairie remains in the northeast where the topography is too rugged for agriculture, and the land is used for grazing. Much of the increase in irrigated cropland in the past two decades in Finney County has been at the expense of the sandsage prairie vegetation community south of the Arkansas River, but two large tracts of prairie remain unbroken. Land-use/land-cover types not in cropland or grassland (woodland, urban, and other developed areas) constitute only 1.2 percent of the total county area.

Finney County was selected for development and testing of the harmonic analysis methodology for several reasons. First, the land use and land cover for the county are well-documented and have been mapped to the level of crop type for 1992 by Egbert *et al.* (1995) (Figure 3). Second, the county contains only a limited number of major crop types, with distinct phenological characteristics (irrigated corn, irrigated alfalfa, winter wheat) and two natural vegetation types (native shortgrass prairie and sandsage prairie). Third, by using the 1992 land-use/land-cover data, large parcels composed of a single crop or land-cover type could be identified as pixels in the AVHRR imagery.

AVHRR Times-Series NDVI Data

NOAA-AVHRR NDVI biweekly composites for 1992 were acquired from the U.S. Geological Survey EROS Data Center in Sioux Falls, South Dakota. Each biweekly composite consists of the maximum NDVI value within each two-week period for each pixel (Eidenshink, 1992). Vegetation index data are rescaled by EROS during processing from a range of −1.0 to +1.0, to 0 to 200. Values less than 100 typically represent snow, ice, water, and other non-vegetated Earth surfaces. Data for Finney County were downloaded from CD-ROMs, were co-registered, and data gaps (missing periods) were identified. Images for missing biweekly composite periods were created by averaging image data for periods bracketing the missing period (e.g., the previous and succeeding periods) (Table 1).

TABLE 1. AVHRR NDVI BIWEEKLY COMPOSITE PERIODS FOR 1992

Period	EROS Composite	Calendar Dates
1	1	10 Jan–23 Jan
2	(Interpolated)	
3	2	31 Jan–13 Feb
4	(Interpolated)	14 Feb–05 Mar
5	3	06 Mar–10 Mar
6	4	20 Mar–02 Apr
7	5	03 Apr–16 Apr
8	6	17 Apr–30 Apr
9	7	01 May–14 May
10	8	15 May–28 May
11	9	29 May–11 Jun
12	10	12 Jun–25 Jun
13	11	26 Jun–09 Jul
14	12	10 Jul–23 Jul
15	13	24 Jul–06 Aug
16	14	07 Aug–20 Aug
17	15	21 Aug–03 Sep
18	16	04 Sep–17 Sep
19	17	18 Sep–01 Oct
20	18	02 Oct–15 Oct
21	19	16 Oct–29 Oct
22	(Interpolated)	30 Oct–12 Nov
23	20	13 Nov–26 Nov
24	(Interpolated)	27 Nov–10 Dec
25	21	11 Dec–24 Dec
26	(Interpolated)	25 Dec–07 Jan 93

Harmonic Analysis

Using the formulas defined above, Fourier coefficients a and b were computed for each term and were then used to calculate the additive term and the amplitudes and phase angles for each of the harmonic components for each pixel in the AVHRR NDVI data set. Images of amplitude and phase angle for each term out to the seventh harmonic term were produced. Given that a time series is the sum of multiple sinusoidal waves, or harmonic terms, the variance of a time series is thus the sum of the variances of the individual terms (Davis, 1986). Percent variance in each image is calculated by first computing the total variance of all terms j in the harmonic analysis using the amplitude values (Davis, 1986): i.e.,

$$Total\ variance = \sum_{1\ to\ n} \frac{(amplitude_j)^2}{2}$$

where j is each term in the series and n is the total number of terms. The percent variance for each term is computed by dividing the individual variance for each term by the total variance. Percent variance was computed on a per-pixel basis to create images of percent variance for each term.

Case Examples

Because farm fields in the Great Plains are smaller than the resolution of the AVHRR sensor, most AVHRR pixels are typically mixtures of two or more different land-use/land-cover types. A method was necessary to identify representative pixels dominated by a single land-cover/land-use type where the phenological response for a pixel as recorded by the AVHRR NDVI time series resulted from predominantly one land-use/land-cover type. Using the 30-meter resolution 1992 land-use/land-cover map produced by Egbert *et al.* (1995), we calculated the percent cover of each land-use/land-cover type within each AVHRR 1000-meter pixel for Finney County, allowing us to identify "pure" pixels composed of a single land-use/land-cover type. Values for amplitude, phase, and percent variance for each term, and the original NDVI value were extracted from the respective images for "pure" pixels for each of the five land-use/land-cover types (corn, winter wheat, alfalfa, grassland, and native sandsage prairie) selected as case examples of the harmonic analysis.

Results and Discussion

Interpretation of the Harmonic Analysis

The additive, or zero term, is the arithmetic mean of NDVI over the time series (26 periods) and represents the overall greenness of a land-cover type, analogous to the first axis of a principal component analysis. Within Finney County, patterns of the additive term generally follow irrigated/non-irrigated land-use patterns (Figure 4a). High values, in particular, irrigated cropland along the Arkansas River, represent high total greenness over the course of a year. Low values (blue and violet) are manifested by land-cover/land-use types that have lower seasonal NDVI values, such as urban areas and the sandsage prairie south of Garden City.

High amplitude values for a given term indicate a high level of variation in temporal NDVI, and the term in which that variation occurs indicates the periodicity of the event. High first-term amplitude values indicate a unimodal temporal NDVI pattern, where a land-use/land-cover has a wide annual range in NDVI values. High amplitude values in the second term indicate semiannual peaks in greenness, a phenomena exhibited in this region by winter wheat. Images of the first- and second-amplitude terms also closely correspond to land-use/land-cover patterns within the study area. The highest first-term amplitude values (white areas on Figure 4b) occur on areas

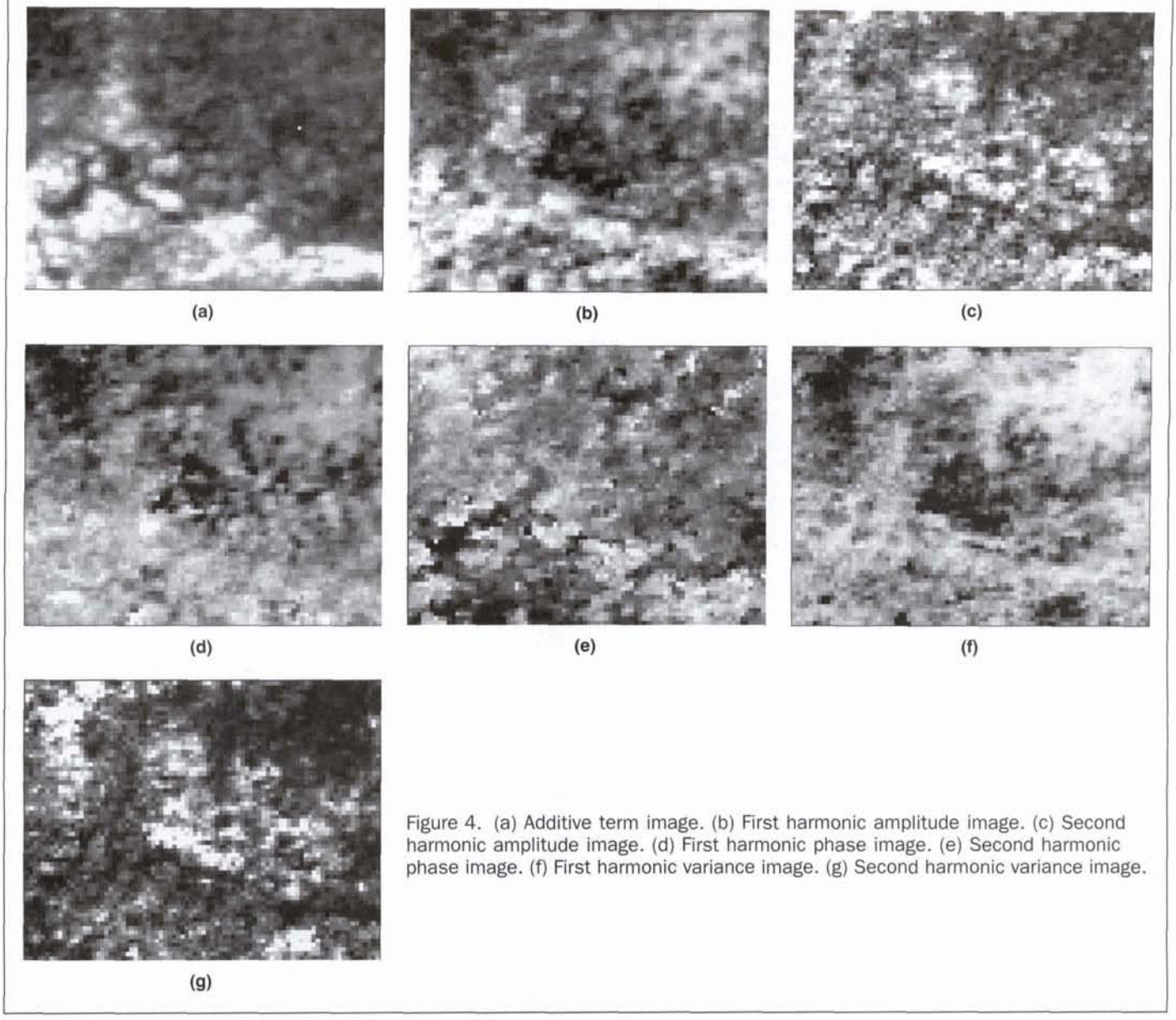

Figure 4. (a) Additive term image. (b) First harmonic amplitude image. (c) Second harmonic amplitude image. (d) First harmonic phase image. (e) Second harmonic phase image. (f) First harmonic variance image. (g) Second harmonic variance image.

planted in corn and alfalfa, while the native grasslands in the northeastern part of the county appear in light grey. Dark tones on the first-term amplitude generally appear white or light grey on the second amplitude image, indicating higher amplitude values in the second term than in the first term (Figure 4c). These are wheat fields or areas in fallow rotation, and exhibit a bimodal temporal NDVI profile as opposed to the unimodal summer peak greenness pattern of corn and alfalfa.

Phase indicates the time of year at which the peak value for a term occurs. For land-use/land-cover types with unimodal NDVI phenological profiles that peak in midsummer (such as irrigated corn or grasslands), phase values typically are near π, or 3.14, over a possible range of 0 to 2π (Table 2). Although grasslands and irrigated cropland in Finney County exhibit different additive term values (Figure 4a) and first-term amplitude values (Figure 4b), first-term phase values are similar, indicating the midsummer peak greenness timing of these cover types (grey areas, Figure 4d). Winter wheat, which dominates the northwestern and central portions of Finney County, appears dark grey to black in Figure 4d, indicating a first-term amplitude peak earlier in the year, consistent with the spring maturing of the winter wheat crop. These concentrations of winter wheat appear light grey to white on the second-term phase image (Figure 4e).

Variance Images

Variance images show the amount of variance in the original data that is contained in a specific harmonic term. As expected, for land-use/land-cover types exhibiting a strongly unimodal NDVI profile, the majority of the variance is contained in the first harmonic term. In Figure 4f, areas where the majority of the variance is contained in the first term appear in white or light grey, and are probably irrigated crops along the Arkansas River in the lower part of the image or native shortgrass prairie in the northeastern corner of the county. Dark areas on Figure 4f indicate that the majority of variance is contained in other terms. Most of the dark areas on Figure 4f appear light on the variance image for the second term (Figure 4g), indicating that these areas are strongly bimodal in their NDVI phenological profile, and are probably winter wheat.

TABLE 2. PARAMETERS OF THE FIRST FOUR HARMONIC FUNCTIONS FOR FIVE LAND-USE/LAND-COVER TYPES

	Term	Amplitude	Phase	*a*	*b*	% Var.	Cum. Var.
Corn	0	125.46					
	1	14.514	3.232	−14.45	−1.31	0.93	0.93
	2	1.806	2.183	−1.04	1.48	0.01	0.94
	3	1.889	0.058	1.89	0.11	0.02	0.97
	4	2.103	0.681	1.63	1.32	0.01	0.98
Shortgrass prairie	0	125.16					
	1	16.067	3.295	−15.88	−2.46	0.93	0.94
	2	2.679	1.850	−0.74	2.57	0.02	0.96
	3	2.450	−0.200	2.40	−0.49	0.01	0.98
	4	1.179	0.033	1.18	0.04	0.00	0.98
Sandsage prairie	0	122.50					
	1	16.059	3.205	−16.03	−1.01	0.90	0.90
	2	2.688	0.740	1.98	1.81	0.00	0.90
	3	1.310	4.679	−0.04	−1.31	0.01	0.92
	4	2.632	0.434	2.39	1.11	0.02	0.94
Alfalfa	0	141.78					
	1	23.146	3.265	−22.97	−2.85	0.84	0.85
	2	6.529	3.289	−6.46	−0.96	0.06	0.92
	3	5.308	0.175	5.23	0.92	0.04	0.96
	4	2.581	−0.120	2.56	−0.31	0.01	0.97
Winter wheat	0	134.02					
	1	7.391	1.977	−2.92	6.79	0.09	0.09
	2	8.915	3.743	−7.35	−5.05	0.55	0.65
	3	1.926	−1.286	0.54	−1.85	0.04	0.69
	4	4.640	1.282	1.32	4.45	0.17	0.86

Case Examples

The following discussion focuses on the best examples of the five land-use/land-cover types to demonstrate and interpret the harmonic analysis technique as applied to time-series satellite imagery. For the purposes of discussion and illustration, data from pixels of exclusively one cover type (i.e, no mixed pixels) are used here. In practice, given the coarse resolution of the AVHRR sensor in relation to the typical field size in the western Great Plains, the NDVI values of most AVHRR pixels are a composite of two or more land-use/land-cover types.

Irrigated Corn

Irrigated corn in Finney County exhibits a strongly unimodal periodic pattern, with a high amplitude value in the first term and low amplitude values in successive terms (Figure 5a). The majority (93 percent) of the total variance in seasonal NDVI is contained in the first harmonic term (Table 2). Peak greenness occurs during mid-summer, as expected for a crop that is planted in the spring, matures by mid-summer, and is harvested by late summer/early fall. In the phenological NDVI profile constructed from summing the additive term and the first four harmonic terms (Figure 5b), the second and third harmonic terms slightly shift the dominant mid-summer (period 13) peak greenness date of the first harmonic term to a later period (period 14, 10–23 July), consistent with typical crop calendars for the region.

Grassland and Sandsage Prairie

Shortgrass prairie grassland and sandsage prairie exhibit a phenological pattern similar to corn in that all three cover types are strongly unimodal, with high first-term amplitude values and the majority of the variance (greater than 90 percent) in the first harmonic term (Figures 6a and 7a). First-term phase values (Table 2) indicate that peak greenness occurs during July, consistent with the warm-season nature of the grass species in both vegetation types. Grassland and sandsage prairie, however, exhibit somewhat different phenological patterns that are a function of the different vegetation occurring in these areas. Sandsage prairie is dominated by sand sagebrush (*Artemisia filifolia* Torr.), interspersed with sand bluestem (*Andropogon hallii* Hack.), little bluestem (*Andropogon scoparius* Michx.), and switchgrass (*Panicum virgatum* L.) and bare soil. Changes in phenological NDVI occur rapidly because these warm-season species increase photosynthetic activity during the spring and early summer, and steadily decline after peaking in mid-July (period 14) (Figure 6b). In contrast, the shortgrass prairie grassland (dominated by buffalograss (*Buchloe dactyloides*), blue grama (*Bouteloua gracilis*), and purple three-awn (*Aristida purpurea* Nutt.) is less constrained in the duration of its growing season and exhibits higher late-summer NDVI than does the sandsage prairie (Figure 7b).

Alfalfa

Alfalfa, although it also exhibits a strong summer-peak greenness pattern, differs from the strongly unimodal pattern of corn and grass in that it has relatively high second-and third-term amplitudes resulting from cultivation practices (Figure 8a). Alfalfa is harvested repeatedly during the summer, producing a secondary and tertiary periodicity in greenness with the growth-cutting-growth-cutting-growth cycle during the summer (Figure 8b). This pattern of greenup-harvest-regrowth-harvest-regrowth is manifested in the harmonic analysis as high additive term values and a strong first harmonic term (85 percent of the total variance is in the first term) (Table 2). Irrigated alfalfa is typically harvested four times in western Kansas during a typical growing season, beginning in May and extending until July-September. Values for variance and amplitude in the second and third terms are substantially higher compared to the variance and amplitude values of respective terms for corn, grass, or sandsage prairie (Table 2).

Wheat

Winter wheat has a strikingly different phenological pattern in comparison to other crop types described above, exhibiting a more bimodal temporal NDVI curve. Winter wheat is planted in the fall (late September/early October), sprouts, and goes dormant over winter and may be covered by snow. In the spring, the wheat greens up and is harvested by May, followed by plowing or fallowing of the land in a two-year or three-year crop rotation. The second harmonic term therefore has the highest

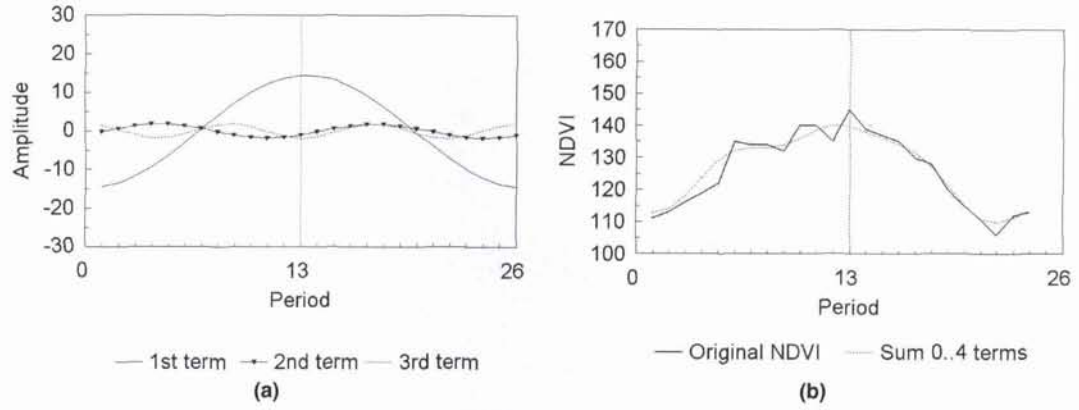

Figure 5. (a) First three harmonic curves for corn. (b) Raw NDVI profile for corn and NDVI profile constructed from the summing the additive term and first four harmonic curves.

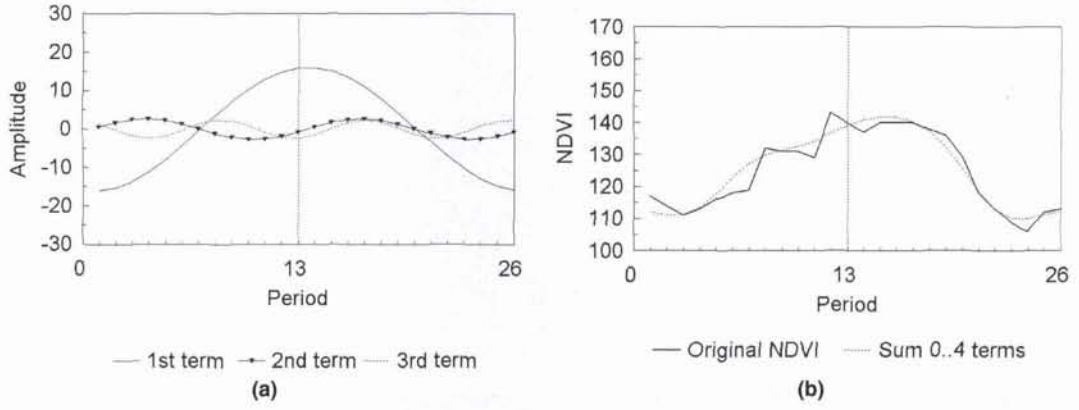

Figure 6. (a) First three harmonic curves for shortgrass prairie grassland. (b) Raw NDVI profile for shortgrass prairie and NDVI profile constructed from the summing the additive term and first four harmonic curves.

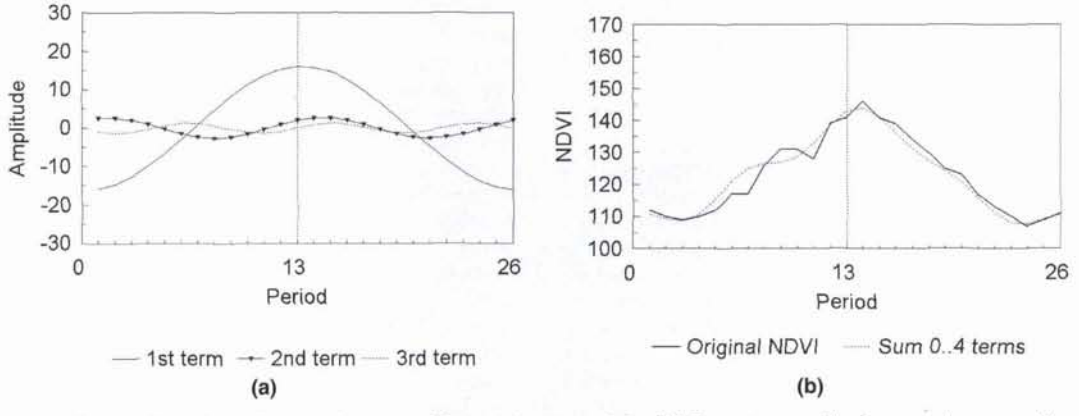

Figure 7. (a) First three harmonic curves for sandsage prairie. (b) Raw NDVI profile for sandsage prairie and NDVI profile constructed from the summing the additive term and first four harmonic curves.

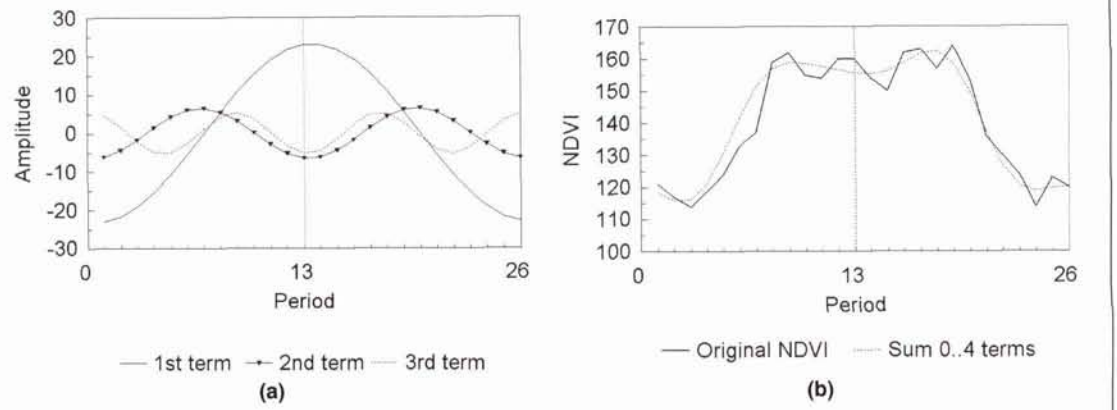

Figure 8. (a) First three harmonic curves for alfalfa. (b) Raw NDVI profile for alfalfa and NDVI profile constructed from the summing the additive term and first four harmonic curves.

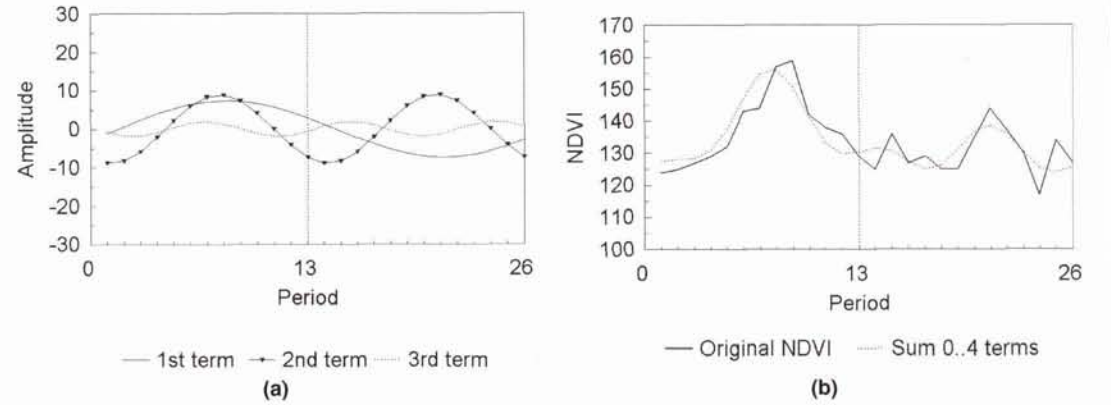

Figure 9. (a) First three harmonic curves for winter wheat. (b) Raw NDVI profile for winter wheat and NDVI profile constructed from the summing the additive term and first four harmonic curves.

amplitude and contains the majority of the variance (Figure 9a), producing the bimodal NDVI profile characteristic of this land-cover type (Figure 9b).

Given that different land-use/land-cover types produce different phase and amplitude values in the harmonic analysis, results suggest that these values of amplitude, phase, and the additive term generated for a single year of time-series data could be used in a cluster analysis for identification and mapping of land-use/land-cover types. Beyond simple characterization and mapping, extension of the harmonic analysis to multiple years of data, applied either on a year-by-year basis or collectively to the entire multiyear data series, may allow the detection of interannual and directional change in land use/land cover. Hobbs (1990) has described several types of vegetation change: (1) seasonal variability, in particular, the phenological change of vegetation throughout the course of a growing season; (2) interannual variability, or change from year to year as a result of climatic variability; and (3) directional vegetation change, which results from intrinsic vegetation processes such as succession, anthropogenic (human-induced) change, or changes in global climatic patterns. Any of the three types of change should be detectable using harmonic analysis of a time-series of satellite imagery by examining changes in amplitude, phase, or the additive term.

What do changes in harmonic parameters (phase and amplitude) for a term over a period of several years imply about changes in the landscape? Changes in seasonal *amplitude* (phase unchanged) may indicate changes in land-use/land-cover type (e.g., changes in a crop type or changes in natural vegetation), or in vegetation condition from drought, flooding, or overgrazing. Changes in *phase* (amplitude unchanged) may indicate changes in time of maximum greenness, which in turn may occur as a result of changes in the onset of greenness, changes in planting time, or changes in the time of harvest. Changes in *both* amplitude and phase over time would be indicative of major and significant changes in land-surface condition. Such radical change could result from postfire regeneration, changes in land management (crop rotation, enrollment in conservation programs), loss of vegetation by natural or anthropogenic disturbance, or changes in regional climate itself driving changes in the vegetation. For example, land management practices such as a two-year crop-fallow rotation pattern should be manifested as high loadings on a bi-annual amplitude term in a two-year series of AVHRR NDVI biweekly composite data.

Harmonic analysis of time-series NDVI data also offers the potential for significant data reduction in that a complex curve can be reconstructed using the additive term and a limited number of terms for phase and amplitude. This paper has shown that nearly all of the variance in the original data (greater than 94 percent) for the four land-use/land-cover classes with unimodal seasonal NDVI trajectories (corn, grassland, alfalfa,

and sandsage prairie) can be accounted for in the first four harmonic terms (Table 2). A curve defined using 26 biweekly NDVI values can thus be mathematically described using nine values instead: the additive term, plus the phase and amplitude values for each of the four terms, or a data reduction of nearly two-thirds. Even for land-use/land-cover types with bimodal seasonal NDVI patterns, such as wheat, the majority of the variance is captured using six harmonic terms, or 13 values, a data reduction of 50 percent.

In contrast to principal components analysis (PCA), another analysis technique often applied to times series data (Eastman and Fulk, 1993; Hirosawa *et al.*, 1996; Jakubauskas *et al.*, 1998), harmonic analysis differs in the manner by which the source data set is analyzed. Harmonic analysis evaluates a time series of imagery on a per-pixel basis, and each pixel is analyzed and coefficients for the transformation are derived independently of other pixels in the data set. Transformations to the data are then applied on a per-pixel basis. Principal component analysis, in contrast, evaluates the variance of all pixels in all images of the time series and includes all pixels in the computation of the transformation coefficients. The PCA transformation to produce derivative components is, however, applied on a per-pixel basis after the coefficients are derived from the entire data set. PCA and the resulting components therefore are biased by the nature of the entire data set (e.g., the range in brightness values, the relative dominance of scene features with differing spectral properties within an image, and the size of an image), while HA does not suffer from any such bias, producing the same values for a pixel independently of the values of other pixels within the image.

The potential of harmonic analysis to act as a noise filter should also be explored as well. Because the noise introduced into an NDVI time series from clouds and processing is non-periodic and infrequent, the harmonic analysis can further serve as a noise reduction technique or filter by using a small number of lower harmonic terms to reconstruct the NDVI profile (Figure 15b). Vegetation phenology patterns, as demonstrated in the above sections, are concentrated in the first three or four harmonic terms, and the high-frequency noise is partitioned into the higher harmonic terms. This potentially obviates the need for data smoothing algorithms that have been applied in other temporal NDVI studies (Reed *et al.*, 1994; Tieszen *et al.*, 1997; Reed and Sayler, 1997).

Conclusions

The objective of this paper was to introduce the use of harmonic, or Fourier, analysis in analyzing time-series satellite imagery, and present several case examples of the technique as applied to several common land-use/land-cover types in the western Great Plains. Although preliminary, the results obtained in the study suggest that there are areas of research and application that could significantly benefit from the use of harmonic analysis in analyzing a time series of satellite remotely sensed imagery. These include land-use/land-cover mapping and monitoring, landscape stability and change analysis, crop type identification, and reduction of data volume and noise in time-series imagery.

Acknowledgments

This research was conducted at the Kansas Applied Remote Sensing (KARS) Program (Edward A. Martinko, Director) at the University of Kansas, Lawrence, Kansas. This research described in this paper was funded by the National Institute for Global Environmental Change (NIGEC), South Central Regional Center at Tulane University (David Sailor, Director), through the U.S. Department of Energy (Cooperative Agreement No. DE-FC03-90ER61010). Any opinions, findings, and conclusions or recommendations expressed in this publication are those of the authors and do not necessarily reflect the views of the DOE.

References

Achard, F., and F. Blasco, 1990. Analysis of vegetation seasonal evolution and mapping of forest cover in West Africa with the use of NOAA AVHRR HRPT data, *Photogrammetric Engineering & Remote Sensing*, 56(10):1359–1365.

Anderson, R.Y., and L.H. Koopmans, 1963. Harmonic analysis of varve time series, *Journal of Geophysical Research*, 68:877–893.

Andres, L., W.A. Salas, and D. Skole, 1994. Fourier analysis of multitemporal AVHRR data applied to a land cover classification, *International Journal of Remote Sensing*, 15(5):1115–1121.

Azzali, S., and M. Menenti, 2000. Mapping vegetation-soil-climate complexes in southern Africa using temporal Fourier analysis using NOAA-AVHRR-NDVI data, *International Journal of Remote Sensing*, 21(5):973–996.

Balling, R.C., 1985. Warm season nocturnal precipitation in the Great Plains of the US, *Journal of Climate and Applied Meteorology*, 24:1383–1387.

Briggs, J., and M.D. Nellis, 1991. Seasonal variation of heterogeneity in the tallgrass prairie: a quantitative measure using remote sensing, *Photogrammetric Engineering & Remote Sensing*, 57(4): 407–411.

Davis, J.C., 1986. *Statistics and Data Analysis in Geology*, Second Edition, J. Wiley and Sons, New York, N.Y., 646 p.

Easterling, D.R., and P.J. Robinson, 1985. The diurnal variation of thunderstorm activity in the United States, *Journal of Climate and Applied Meteorology*, 24:1048–1058.

Eastman, J.R., and M. Fulk, 1993. Long sequence time series evaluation using standardized principal components, *Photogrammetric Engineering & Remote Sensing*, 59(8):1307–1312.

Egbert, S.E., K.P. Price, M.D. Nellis, and R. Lee, 1995. Developing a land cover modeling protocol for the High Plains using multiseasonal Thematic Mapper imagery, *Proceedings of the 1995 ASPRS/ACSM Annual Meeting*, 27 February–02 March, Charlotte, North Carolina, pp. 836–845.

Eidenshink, J.C., 1992. The 1990 conterminous U.S. AVHRR data set, *Photogrammetric Engineering & Remote Sensing*, 58(6):809–813.

Hamilton, K., 1981. A note on the observed diurnal and semidiurnal rainfall variations, *Journal of Geophysical Research*, 86:12,122–12,126.

Heddinghaus, T.R., and E.C. Kung, 1980. An analysis of climatological patterns of the northern hemisphere circulation, *Monthly Weather Review*, 108(1):1–17.

Hirosawa, Y., S.E. Marsh, and D.H. Kliman, 1996. Application of standardized principal component analysis to land-cover characterization using multitemporal AVHRR data, *Remote Sensing of Environment*, 58:267–281.

Hobbs, R.J., 1990. Remote sensing of spatial and temporal dynamics of vegetation, in *Remote Sensing of Biosphere Functioning* (R.J. Hobbs and H.A. Mooney, editors), Springer-Verlag, New York, N.Y., pp. 203–219.

Horn, L.H., and R.A. Bryson, 1960. Harmonic analysis of the annual march of precipitation over the United States, *Annals of the Association of American Geographers*, 50(2):157–171.

Jakubauskas, M.E., K. Kindscher, and D. Debinski, 1998. Multitemporal characterization and mapping of montane sagebrush communities using Indian IRS LISS-II imagery, *Geocarto International*, 13(4):65–74.

Jensen, J.R., 1996. *Introductory Digital Image Processing, Second Edition*, Prentice-Hall, Engelwood Cliffs, New Jersey, 316 p.

Kastens, D.L., K.P. Price, E.A. Martinko, and T.L. Kastens, 1998. Assessing Wheat Conditions in Kansas Using Biweekly AVHRR Datasets and Crop Phenological Indices, *Proceedings, First International Conference on Geospatial Information in Agriculture and Forestry*, 01–03 June, Lake Buena Vista, Florida, pp. II-538–II-544.

Kremer, R.G., and S.W. Running, 1993. Community type differentiation using NOAA/AVHRR data within a sagebrush-steppe ecosystem, *Remote Sensing of Environment*, 46:311–318.

Lancaster, J., D. Mouat, R. Kuehl, W. Whitford, and D. Rapport, 1996. Time series satellite data to identify vegetation response to ecosystem stress as an indicator of ecosystem health, *Proceedings,*

Shrubland Ecosystem Dynamics in a Changing Environment, 23–25 May 1995, Las Crucas, New Mexico, General Technical Report INT-GTR-338, U.S. Department of Agriculture, Forest Service, Intermountain Research Station, Ogden, Utah, pp. 255–261.

Landin, M.G., and L.F. Bosart, 1985. Diurnal variability of precipitation in the northern United States, *Monthly Weather Review*, 113:989–1014.

———, 1989. The diurnal variation of precipitation in California and Nevada, *Monthly Weather Review*, 117:1801–1816.

Legates, D.R., and C.J. Willmott, 1990a. Mean seasonal and spatial variability in gauge-corrected, global precipitation, *International Journal of Climatology*, 10(2):111–127.

———, 1990b. Mean seasonal and spatial variability in global surface air temperature, *Theoretical and Applied Climatology*, 41(1): 11–21.

Lloyd, D., 1990. A phenological classification of terrestrial vegetation cover using shortwave vegetation index imagery, *International Journal of Remote Sensing*, 11(12):2269–2279.

Loveland, T., J. Merchant, J.F. Brown, D.O. Ohlen, B. Reed, P. Olson, and J. Hutchinson, 1995. Seasonal land-cover regions of the United States, *Annals of the Association of American Geographers*, 85(2):339–355.

Masò, C., 1991. *Use of Satellite Imagery in the Investigation of Warm Season Thunderstorm Precipitation*, M.A. Thesis, University of Oklahoma, Norman, Oklahoma, 134 p.

Myneni, R.B., C.D. Keeling, C.J. Tucker, G. Asrar, and R.R. Nemani, 1997. Increased plant growth in the northern high latitudes from 1981 to 1991, *Nature*, 386:695–702.

Olsson, L., and L. Eklundh, 1994. Fourier series for analysis of temporal sequences of satellite sensor imagery, *International Journal of Remote Sensing*, 15(18):3735–3741.

Rasmusson, E.M., 1971. *Diurnal Variation of Summertime Thunderstorm Activity over the United States*, Technical Note 71-4, U.S. Air Force Environmental Technical Applications Center, Washington, D.C., 12 p.

Rayner, J.N., 1971. *An Introduction to Spectral Analysis*, Pion Ltd., London, 174 p.

Reed, B., J. Brown, D. VanderZee, T. Loveland, J. Merchant, and D.O. Ohlen, 1994. Measuring phenological variability from satellite imagery, *Journal of Vegetation Science*, 5:703–714.

Reed, B.C., T. Loveland, and L.L. Tieszen, 1996. An approach for using AVHRR data to monitor US Great Plains grasslands, *Geocarto International*, 11:13–22.

Reed, B.C., and K. Sayler, 1997. A method for deriving phenological metrics from satellite data, Colorado 1991–1995, *Proceedings, Internet Workshop on Impact of Climate Change and Land Use on the Southwestern United States*, 07–25 July, online http://geochange.er.usgs.gov/sw/

Reed, B.C., and L. Yang, 1997. Seasonal vegetation characteristics of the United States, *Geocarto International*, 12(2):65–71.

Riley, G.T., M.G. Landin, and L.F. Bosart, 1987. The diurnal variability of precipitation across the central Rockies and adjacent Great Plains, *Monthly Weather Review*, 115:1161–1172.

Roller, N.E., and J.E. Colwell, 1986. Coarse-resolution satellite data for ecological surveys, *BioScience*, 36(7):468–475.

Samson, S.A., 1993. Two indices to characterize temporal patterns in the spectral response of vegetation, *Photogrammetric Engineering & Remote Sensing*, 59(4):511–517.

Schowengerdt, R.A., 1997. *Remote Sensing: Models and Methods for Image Processing*, Academic Press, San Diego, California, 522 p.

Schulz, M., and K. Stattegger, 1997. Spectral analysis of unevenly spaced paleoclimatic time series, *Computers and Geosciences*, 23:929–945.

Tieszen L., B. Reed, N. Bliss, B. Wylie, and D. DeJong, 1997. NDVI C3 and C4 production and distributions in Great Plains grassland cover classes, *Ecological Applications*, 7:59–78.

Tucker, C.J., C.L. Vanpraet, M.J. Sharman, and G. Van Ittersum, 1985. Satellite remote sensing of total herbaceous biomass production in the Senglade Sahel: 1980–1984, *Remote Sensing of Environment*, 17:233–249.

van Loon, H., R.L. Jenne, and K. Labitzke, 1973. Zonal harmonic standing waves, *Journal of Geophysical Research*, 78(21):4463–4471.

Verhoef, W., M. Menenti, and S. Azzali, 1996. A colour composite of NOAA-AVHRR-NDVI based on time series analysis (1981–1992), *International Journal of Remote Sensing*, 17(2):231–235.

Wallace, J.M., 1975. Diurnal variation in precipitation and thunderstorm frequency over the conterminous United States, *Monthly Weather Review*, 103:406–419.

Yevjevich, V., 1972. *Stochastic Processes in Hydrology*, Water Resources Publications, Ft. Collins, Colorado, 276 p.

(Received 30 November 1999; revised and accepted 15 June 2000)